6720 J. Med. Chem. 2010, 53, 6720–6729
DOI: 10.1021/jm100839w

Journal of Medicinal Chemistry Article

Potent and Fully Noncompetitive Peptidomimetic Inhibitor of Multidrug Resistance P-Glycoprotein

Ophélie Arnaud,[†,⊥] Ali Koubeissi,[‡,⊥] Laurent Ettouati,*[,‡] Raphaël Terreux,[†] Ghina Alamé,[§] Catherine Grenot,[§] Charles Dumontet,[∥] Attilio Di Pietro,[†] Joëlle Paris,[‡] and Pierre Falson*[,†]

[†]*Laboratoire des Protéines de Résistance aux Agents Chimiothérapeutiques, Equipe Labellisée Ligue 2009, Institut de Biologie et Chimie des Protéines, UMR 5086 CNRS, Université Lyon 1, IFR 128 BioSciences Gerland Lyon-Sud, F-69367 Lyon, France,* [‡]*EA 3741 Écosystèmes et Molécules Bioactives, Institut des Sciences Pharmaceutiques et Biologiques, Université de Lyon, Université Claude Bernard Lyon 1, F-69373 Lyon, France,* [§]*Université de Lyon, Université Claude Bernard Lyon 1, INSERM, U863, F-69373 Lyon, France, and* [∥]*Laboratoire de Cytologie Analytique, Faculté de Médecine, Université de Lyon, Université Claude Bernard Lyon 1, INSERM U590, F-69373 Lyon, France.*
[⊥] *Co-first-authors.*

Received July 6, 2010

N^{α}-Boc-L-Asp(OBn)-L-Lys(Z)-O*t*Bu (reversin 121, **1**), an inhibitor of the P-gp ABC transporter, was used to conceive compounds inhibiting the drug efflux occurring through the Hoechst 33342 and daunorubicin transport sites of P-gp, respectively H and R sites. Replacement of the aspartyl residue by *trans*-4-hydroxy-L-proline (4(*R*)Hyp) gave compounds **11** and **15** characterized by half-maximal inhibitory concentrations (IC_{50}) of 0.6 and 0.2 μM, which are 2- and 7-fold lower than that of the parent molecule. The difference in IC_{50} between **11** and **15** rests on the carbonyl group of the peptidyl bond, reduced in **15**. Those compounds are rather specific of P-gp, having no or limited activity on MRP1 and BCRP. **15** displayed no marked cytotoxicity up to 10-fold its IC_{50}. Importantly, **15** equally inhibited the Hoechst 33342 and daunorubicin effluxes through a typical noncompetitive inhibition mechanism, suggesting its binding to a site different from the H and R drug-transport sites.

Introduction

ABC[a] (ATP-binding cassette) transporters constitute a key family[1] in the field of public health. Proteins of this family are involved in several genetic diseases[2] and are responsible for the cellular multidrug resistance phenotype encountered during chemotherapeutic treatments against cancer and viral diseases.[3−5] In such a context, they represent a serious threat, since cancer cells overexpress them to reduce drug concentration below its cytotoxic threshold. Three ABC transporters are mainly responsible for this phenomenon: P-glycoprotein (P-gp/ABCB1), which was the first identified protein involved in drug resistance[6] and remains the major agent involved in this phenomenon; the multidrug resistance protein (MRP1/ABCC1), involved in cells where P-gp is not overexpressed;[7] the breast cancer resistance protein (BCRP/ABCG2).[8,9] Drug resistance driven by these membrane proteins is emphasized first by their intrinsic polyspecificity, with these pumps transporting a wide spectrum of molecules, and second by common structural characteristics of their drug-binding sites.

Four sites have been described for the binding of drugs and modulators within P-gp[10,11] (see also the recent review of Colabufo and colleagues[12]). This suggests a large binding pocket, as early modeled in silico by Garrigos and Orlowski,[13] and recently experimentally observed by Chang and colleagues by resolving the 3D structure of the mouse P-gp homologue[14] which displays a volume of 6000 Å^3. Among these sites, two drug-binding regions have been functionally identified: one site called "R" from its capacity to bind rhodamine 123 and anthracyclines, such as doxorubicin or daunorubicin, and a second one called "H", which binds Hoechst 33342, colchicine, and quercetin.[15] Shapiro and Ling observed that these drug-binding sites are distinct and are characterized by a positive cooperativity, although they can partially overlap, since rhodamine 123 above 2 μM quantitatively reduces Hoechst 33342 binding.[15]

Numerous multidrug-resistance reversing agents have been described since the discovery of verapamil.[16,17] Among them, peptides are quite scarce. Valspodar/SDZ-PSC-833, a cyclosporin A derivative, is the best representative of compounds that have ultimately reached phase III clinical trials but were stopped because of pharmacokinetic interactions with anticancer drugs and/or lack of specificity.[18] Two hexacyclic peptides, QZ59-SSS and QZ59-RRR, were recently cocrystallized with the mouse P-gp.[14] Besides these relatively large molecules, a series of short peptide P-gp inhibitors called reversins was first described by Seprõdi and colleagues.[19,20] They consist of di- and tripeptide derivatives sharing common physicochemical and structural features, such as bulky aromatic and/or alkyl groups. Among them, **1** (reversin 121) is an aspartyllysine (Asp-Lys) dipeptide derivative displaying good affinity and specificity for P-gp.[21]

The present work describes a novel class of P-gp ligands, of which the most potent, **15**, behaves as a noncompetitive inhibitor for both the R and H drug-transport sites of P-gp,

*To whom correspondence should be addressed. For L.E.: phone, +33 (0)47 877 7082; fax, +33 (0)47 877 7082; e-mail, laurent.ettouati@univ-lyon1.fr. For P.F.: phone, +33 (0)43 765 2916; fax, +33 (0)47 272 2604; e-mail, p.falson@ibcp.fr.

[a] Abbrevations: ABC, ATP-binding cassette; P-gp/ABCB1, P-glycoprotein; MRP1/ABCC1, multidrug resistance protein 1; BCRP/ABCG2, breast cancer resistance protein; LDA, lithium diisopropylamide; THF, tetrahydrofuran; Z, benzyloxycarbonyl; 3D-QSAR, 3D quantitative structure−activity relationship; CoMSIA, comparative molecular similarity indices analysis; LOO, leave one out; Bn, benzyl.

 Published on Web 08/23/2010

Table 1. First Series of Reversin Derivatives and P-Gp Modulation Activity

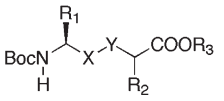

						NIH3T3 transfected cells			K562/R7 resistant cells
compd	R_1	X	Y	R_2	R_3	% inh eff[a] (10 μM)	% inh eff[a] (2 μM)	IC_{50}, μM	% inh eff[a] (10 μM)
1	-CH_2COOBn	C=O	NH	(*S*)-$(CH_2)_4$-NHZ	^{t}Bu	75.8 ± 1.6		1.41 ± 0.34	88.0 ± 0.6
30	-CH_2COOBn	C=O	CH_2	(*S*)-$(CH_2)_4$-NHZ	Bn	35.7 ± 15.3			
17	-CH_2COOBn	ψ(CO-CH_2)-Gly		(*S*)-$(CH_2)_4$-NHZ	^{t}Bu	67.7 ± 7.0			
2	-$(CH_2)_2$COOBn	C=O	NH	(*S*)-$(CH_2)_4$-NHZ	^{t}Bu	63.7 ± 5.4			
3	-$(CH_2)_2$COO^{t}Bu	C=O	NH	(*S*)-$(CH_2)_4$-NHZ	^{t}Bu	37.2 ± 13.7			
7	-$(CH_2)_3$COOBn	C=O	NH	(*S*)-$(CH_2)_4$-NHZ	^{t}Bu	97.8 ± 4.0	37.0 ± 9.0		65.5 ± 1.3
4	-$(CH_2)_2$OCOBn	C=O	NH	(*S*)-$(CH_2)_4$-NHZ	^{t}Bu	59.6 ± 14.7			
5	-$(CH_2)_2$OCOcHex	C=O	NH	(*S*)-$(CH_2)_4$-NHZ	^{t}Bu	61.8 ± 3.2			
8	-$(CH_2)_3$OCOcHex	C=O	NH	(*S*)-$(CH_2)_4$-NHZ	^{t}Bu	82.3 ± 1.9	35.7 ± 15.2		80.4 ± 4.5
6	-$(CH_2)_2$OBn	C=O	NH	(*S*)-$(CH_2)_4$-NHZ	^{t}Bu	49.2 ± 10.2			
13	-CH_2*p*-PhO^{t}Bu	C=O	NH	(*S*)-$(CH_2)_4$-NHZ	^{t}Bu	34 ± 10.6			
16	-CH_2*p*-PhO^{t}Bu	CH_2	NH	(*S*)-$(CH_2)_4$-NHZ	^{t}Bu	49.1 ± 5.8			
14	-CH_2*p*-PhO^{t}Bu	C=O	NH	H	^{t}Bu	93.4 ± 13.3	38.0 ± 7.2		
19	-CH_2*p*-PhO^{t}Bu	C=O	(*RS*)$CHSO_2$Ph	H	^{t}Bu	106.5 ± 8.6		1.55 ± 0.86	
20	-CH_2*p*-PhO^{t}Bu	(*RS*)CHOH	(*RS*)$CHSO_2$Ph	H	^{t}Bu	104.4 ± 10.4			
21	-CH_2*p*-PhO^{t}Bu	ψ(*E*,CH=CH)		H	^{t}Bu	71.2 ± 1.5			
22	-CH_2*p*-PhO^{t}Bu	CH_2	CH_2	H	^{t}Bu	78.7 ± 8.3			

[a] The efficacy of inhibition of drug efflux mediated by P-gp (% inh eff) is indicated, estimated as described in the Experimental Section from NIH3T3 mouse cells expressing specifically P-gp or human K562/R7 drug resistant cell line[32] which mainly expresses P-gp, and for selected compounds the same experiment was carried out with HEK 293 and BHK expressing BCRP and MRP1, respectively. The efficacy of inhibition was initially measured at 10 μM of each compound and then at 2 μM for those displaying 80% efficacy at 10 μM. The concentration of half maximal inhibition, IC_{50}, was estimated for the most potent compounds as detailed in caption of Figure 1. All data are the mean of duplicate experiments carried out twice.

which limits the possibility for such an inhibitor to be itself transported by P-gp or another ABC transporter. We chose **1** as a starting template, modified the aspartic acid side chain length and ester-protecting group, then replaced the aspartic acid residue by side chain constrained derivatives, and finally modified the peptide bond. We also evaluated the inhibitory effect of tyrosylglycine dipeptide derivatives closely related to **1**, especially concerning the hydrophobic protecting groups. Once generated, these derivatives were assayed in vitro, looking for compounds displaying a better inhibition efficacy than **1** and, among them, selecting those behaving as noncompetitive inhibitors for the H and R sites.

Results and Discussion

Chemistry. The products described in this article and presented in Tables 1−4 were synthesized by standard procedures.[22,23] Reference reversins **1** and N^{α}-Boc-L-Glu-(OBn)-L-Lys(Z)-O^{t}Bu (reversin 1092, **2**), as well as other dipeptide derivatives **3**−**14**, were obtained by the mixed anhydride method (Tables 1 and 2).[24] Aminomethylene derivatives **15** and **16** were synthesized using the classical reductive amination strategy, starting from chiral pool-derived aminoaldehydes (Tables 1 and 2).[25] Synthesis of ketomethylene derivative **17**, bearing a Gly residue inserted between Asp and Lys residues, was previously reported, as well as the synthesis of β-ketosulfone **18**,[23] Tyr-Gly derivatives **19**−**22**,[23] and derivatives of (2*S*)-[3-((1*S*),3-bis-benzyloxycarbonylpropylcarbamoyl)propionylamino]pentanedioic acid dibenzyl ester (reversin 213, **23**) and **24**[22] (Tables 1, 3, and 4). To obtain further information on the peptide bond effect on the activity of **1**, we synthesized its ketomethylene derivative **30** (Scheme 1) using a strategy developed by Hoffman and Tao.[26] This strategy implies the condensation of an amino acid derived β-keto enolate with an amino acid derived 2-triflyloxy ester, giving rise to the corresponding ketomethylene. It is stressed that triflyloxy ester synthesis undergoes a configuration inversion. However, for the sake of economy and development, L-lysine was used instead of its enantiomer (Scheme 1). The aspartic acid derived β-keto ester **25** was obtained in 32% yield by reaction of aspartic acid imidazolyl ester with the allyl acetate derived enolate generated by the reaction with LDA and allyl acetate in THF. Unexpectedly, the allyl ester byproduct **26** was also recovered in 21% yield. Concerning the synthesis of the L-lysine-derived 2-triflyloxy ester **29**, the Z-protected L-lysine-derived α-hydroxy acid **27** was obtained in quantitative yield by treatment of Z-protected L-lysine with sodium nitrite in 50% aqueous acetic acid.[27] We chose a benzyl protection group for the carboxylic acid of **27**, as *tert*-butyl protection would imply a lengthy procedure.[28] Finally we prepared the unstable triflyloxy ester **29** in 41% yield, according to the method of Weber et al.[29] Coupling of protected triflyloxy ester **29** with aspartic acid derived β-keto ester **25** was carried out in THF with sodium hydride as base for 3 h at room temperature, and then the crude adduct was treated with Pd(0) to finally obtain the ketomethylene derivative **30** in 26% overall yield.[30]

Biological Results. The efficacy of the compounds to prevent the daunorubicin, mitoxantrone, and Hoechst 33342 efflux carried out by P-gp was evaluated by flow cytometry. The amount of a fluorescent anticancer drug substrate remaining in the cell was quantified in MDR1-transfected NIH3T3/P-gp cell line expressing P-gp, and a P-gp-positive drug-selected human leukemic K562/R7 resistant cell line. The former cellular model has the advantage to selectively express P-gp while the latter one is a biological

Table 2. Second Series of Reversin Derivatives and P-gp Modulation Activity

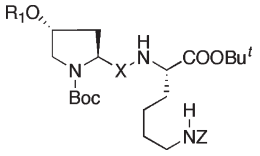

			NIH3T3 P-gp transfected cells			K562/R7 resistant cells	HEK293 BCRP transfected cells	BHK MRP1 transfected cells
compd	R_1	X	% inh eff[a] (10 μM)	% inh eff[a] (2 μM)	IC_{50}, μM	% inh eff[a] (10 μM)	% inh eff[a] (10 μM)	% inh eff[a] (10 μM)
9	COBn	C=O	68.2 ± 10.2			88.2 ± 5.1	10.0 ± 7.5	
15	Bn	CH_2	106.9 ± 23.0		0.22 ± 0.03	77.6 ± 1.5	42.3 ± 0.8	9.0 ± 3.5
10	COcHex	C=O	105.7 ± 13.4		1.68 ± 0.28	94.9 ± 0.4	11.2 ± 4.6	
11	Bn	C=O	99.7 ± 11.0	120.5 ± 35.3	0.73 ± 0.20	83.5 ± 3.0	16.6 ± 3.4	7.0 ± 2.0
12	CH_2cHex	C=O	76.6 ± 10.1	82.2 ± 10.8	1.13 ± 0.34	79.8 ± 1.2	18.8 ± 10.0	

[a] The efficacy of inhibition of drug efflux mediated by P-gp (% inh eff) is indicated, estimated as described in the Experimental Section from NIH3T3 mouse cells expressing specifically P-gp or human K562/R7 drug resistant cell line[32] which mainly expresses P-gp, and for selected compounds the same experiment was carried out with HEK 293 and BHK expressing BCRP and MRP1, respectively. The efficacy of inhibition was initially measured at 10 μM of each compound and then at 2 μM for those displaying 80% efficacy at 10 μM. The concentration of half maximal inhibition, IC_{50}, was estimated for the most potent compounds as detailed in caption of Figure 1. All data are the mean of duplicate experiments carried out twice.

Table 3. Third Series of Reversin Derivatives and P-gp Modulation Activity

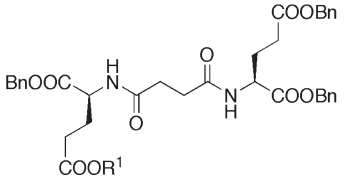

		NIH3T3 P-gp transfected cells
compd	R_1	% inh eff[a](10 μM)
23	Bn	26.6 ± 7.7
24	cHex	29.3 ± 12.3

[a] The efficacy of inhibition of drug efflux mediated by P-gp (% inh eff) is indicated, estimated as described in the Experimental Section from NIH3T3 mouse cells expressing specifically P-gp or human K562/R7 drug resistant cell line[32] which mainly expresses P-gp, and for selected compounds the same experiment was carried out with HEK 293 and BHK expressing BCRP and MRP1, respectively. The efficacy of inhibition was initially measured at 10 μM of each compound and then at 2 μM for those displaying 80% efficacy at 10 μM. The concentration of half maximal inhibition, IC_{50}, was estimated for the most potent compounds as detailed in caption of Figure 1. All data are the mean of duplicate experiments carried out twice.

Table 4. Derivative **18** and P-gp Modulation Activity

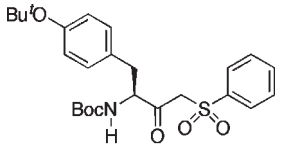

18

	NIH3T3 P-gp transfected cells
compd	% inh eff[a](10 μM)
18	49.1 ± 8.8

[a] The efficacy of inhibition of drug efflux mediated by P-gp (% inh eff) is indicated, estimated as described in the Experimental Section from NIH3T3 mouse cells expressing specifically P-gp or human K562/R7 drug resistant cell line[32] which mainly expresses P-gp, and for selected compounds the same experiment was carried out with HEK 293 and BHK expressing BCRP and MRP1, respectively. The efficacy of inhibition was initially measured at 10 μM of each compound and then at 2 μM for those displaying 80% efficacy at 10 μM. The concentration of half maximal inhibition, IC_{50}, was estimated for the most potent compounds as detailed in caption of Figure 1. All data are the mean of duplicate experiments carried out twice.

model close to an in vivo chemoresistance phenotype. All drugs were assayed at 10 μM in the NIH3T3 cells, and the most efficient ones were then tested in K562/R7 cells. Compounds displaying more than 80% efficacy were assayed at 2 μM, and the half-maximal inhibition concentration, IC_{50}, was determined for the most active ones. A typical experiment is displayed in Supporting Information Figure SI 1 to detail the experimental procedure. As shown, values obtained with NIH3T3/P-gp cells can be higher than those obtained with control cells (see panel C, at 0.8 and 1 μM **15**), giving a higher level of variability than observed with the K562/R7 resistant cells. Transfected cells were used to compare all compounds, as they express a unique transporter. The reference compound **1** (Table 1), developed by Sarkadi and colleagues,[21] displayed 75% inhibition at 10 μM in our transfected-cell system, corresponding to an IC_{50} of 1.41 μM, a value close to the 88% obtained when using the drug-resistant cell lines. Few compounds displayed an efficacy below 40%, such as **30**, **3**, **13** (Table 1), and **23**, **24** (Table 3), whereas most of them such as **2**, **17**, **4**, **5**, **16**, **21**, **22** (Table 1), **12** (Table 2), and **18** (Table 4) displayed an efficacy similar to that of **1**. Finally, nine dipeptides were found to be more efficient than **1**: **7**, **8**, **14**, **19**, **20** (Table 1), and most of the compounds of Table 2 (**9**, **15**, **10**, **11**). Efficacies obtained from drug-selected cells were in the same range (Tables 1 and 2), showing that those compounds remain efficient in a system closer to a physiopathological context than transfected cells.

Structure−Activity Relationships. Several modifications had no positive effect or were negative, e.g., replacement of the amide bond by a ketomethylene isostere in **30** or extension of the aspartate side chain in **2** and **7**. Extending the length of the aspartate side chain slightly increased the efficacy of **7**, which however remained poorly active at 2 μM.

Scheme 1. Synthesis of Ketomethylene Isostere **30**[a]

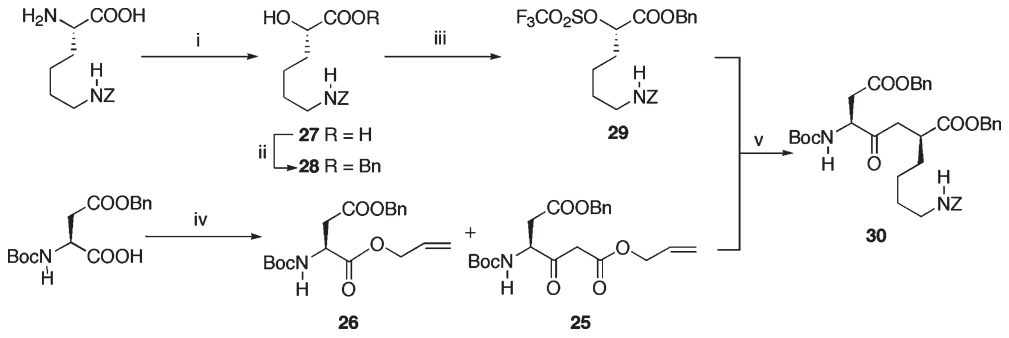

[a] Reagents and conditions: (i) (a) 50% aqueous acetic acid, room temp; (b) $NaNO_2$, H_2O, room temp, quant yield; (ii) BnBr, Et_3N, acetone, room temp, 6 h, 40%; (iii) Tf_2O, CH_2Cl_2, 2,6-lutidine, −78 °C, 4 h, to room temp, 41%; (iv) (a) CDI; (b) CH_3CO_2allyl, LDA, THF, −78 °C, 2 h, **25** 32% and **26** 21%; (v) (a) NaH, THF, −20 °C, 20 min, to room temp, 3 h; (b) $Pd(OAc)_2$, PPh_3, HCOOH, Et_3N, THF, room temp, 24 h, 26%.

In a similar manner, derivatives obtained from **2**, in which the protecting group of the Asp carboxyl side chain was replaced by a *tert*-butyl in **3** or in which the ester was replaced by a reversed ester in **4**, **5**, and **8** or by a benzyl ether in **6**, were not more efficient than **1**.

In another set of modifications, we replaced the aspartyl residue by a tyrosine. This single replacement reduced the overall efficacy of resulting reversins **13** and **16** to 34%, whereas a surprising increase to about 100% was obtained by additionally replacing the lysine moiety by a (*RS*)$CHSO_2$-$PhCH_2$ group. In this series, the most efficient derivative, **19**, led to an IC_{50} of 1.55 μM, similar to that of **1**. A deep reduction in efficacy was also observed for lengthened derivatives **23** and **24** (Table 3).

Conversely, striking effects were also observed by introducing a higher level of constraint in template **2**, e.g., replacing the N-terminal Glu residue by 4(*R*)Hyp residue, resulting in the products listed in Table 2. Apart from **9**, compounds of that series displayed an inhibition efficacy at 10 μM close to 100%, leading to IC_{50} values of 1.68, 1.13, 0.73, and 0.22 μM for **10**, **12**, **11**, and **15**, respectively. As shown in Table 2, some of these improvements were due to the replacement of the ester function of the N-terminal residue by either a benzyl ether function in **11** and **15** or cyclohexylmethylene ether in **12**. A significant improvement was obtained by a single reduction of the peptide bond in **15**, compared to **11**, allowing it to reach the highest affinity with an IC_{50} of 0.22 μM. This value is nearly 1 order of magnitude lower than that of template **1** (Figure 1).

A 3D quantitative structure−activity relationships (3D-QSAR) analysis was then carried out on the reversin derivatives. As detailed in the Experimental Section, models were first energetically minimized and chains were then drawn in a linear conformation. Since those molecules have a great degree of freedom, a linear conformation was chosen for all of them. They were first aligned on the peptide backbone, and then alignment of each side chain was manually carried out by rotating dihedral angles. Each model was then minimized, setting the upper energy threshold to 20 kcal·mol^{-1}. The resulting alignment is displayed in Figure 2A. A database was generated from all models and treated by the CoMSIA method to carry out 3D-QSAR studies (see Experimental Section for details). Values of inhibition efficacy measured at 10 μM of each compound from Tables 1−4 were used for calculations with the LOO (leave one out) cross-validation method. The plot of predicted vs observed inhibitions values is shown in Figure 2B (close circles), with a linear correlation coefficient q^2 of 0.85, indicating that 3D-QSAR calculations were robust enough to give an accurate prediction of the percent inhibition by a candidate molecule. Isopotential volumes of hydrophobic, electrostatic, and steric fields were drawn as displayed in Figure 2, panels C and D. Analysis of the hydrophobic field (panel C) showed that this character is mainly favored (pink grids) at the vicinity of the phenyl moiety of the Z protecting group, associated with a favorable steric hindrance (panel D, yellow grids). This illustrates the importance of bulky nonpolar protecting groups in this area. A small unfavorable hydrophobic region can be observed close to the Z carbamate group (panel C, black grids), coupled with a sterically favorable region that might be ascribed to HB-acceptor interactions with polar P-gp residues. By contrast, the region encompassing the N-terminal Boc carbamate group appears hydrophobically favorable and sterically unfavorable (pink and green grids, respectively). The same trend is observed for the C-terminal *tert*-butyl region, suggesting that in both cases the local docking pockets of these groups should be hydrophobic and of small size. Region (I) is hydrophobically unfavorable and sterically favorable (black and yellow grids, respectively), suggesting that it should not contain large hydrophobic groups, as those introduced in **23** and **24**. As displayed in panel D, an electrostatic field appears unfavorable (blue grids) at the vicinity of the backbone NH group but favorable (red grids) in the background, which could be ascribed to the positive effects observed with the sulfone-containing compound **18**. Such an electrostatic contribution, limited to the peptide backbone and associated with the global hydrophobic character of the inhibitor, suggests that the corresponding hydrophilic volume could be embedded in a hydrophobic environment and that the inhibitor could bind to a hydrophobic pocket. Region II, at the level of the benzyl-protecting group (Bn), appears hydrophobically unfavorable and sterically favorable (black and yellow grids, respectively), which could illustrate the positive impact of ester bridge shift on the inhibition activity.

Specificity, Reversing Efficacy, and Toxicity of Peptides Derivatives. The compounds listed in Table 2 produced only low or even no inhibition of BCRP/ABCG2 and MRP1/ABCC1 when tested at 10 μM on cells expressing those ABC transporters. They thus appear rather specific toward P-gp. This is useful for preserving the physiological activity of ABC transporters not concerned by the drug resistance.

We then characterized the inhibition properties of the most active compound **15**. As shown in Figure 3, the specific expression of P-gp in NIH3T3 cells led to a resistance index of 8.5 for daunorubicin (circles vs triangles) that remains limited but significant enough to observe a further sensitization effect. Further addition to this drug-resistant cell line of 1 μM **15**, corresponding to 5-fold its IC_{50}, restored its initial sensitivity to the anticancer drug (diamonds), showing the efficacy of **15** to reverse the drug resistance phenotype. At this concentration, no marked cytotoxicity was observed as shown in Figure 4. Indeed, viability of either cell expressing P-gp (squares) or control ones (circles) was not significantly altered up to 1 μM. A much pronounced toxicity was, however, observed above 2 μM, a concentration that is 10 times higher than the corresponding IC_{50}.

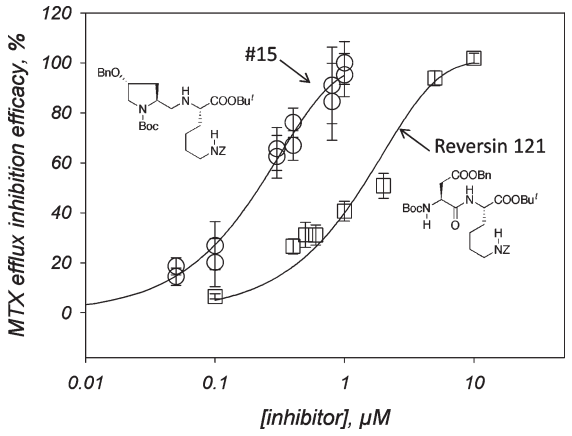

Figure 1. Reversion of P-gp-mediated mitoxantrone efflux by **1** and **15**. The inhibition efficacy of peptide derivatives was assayed by flow cytometry, quantifying the intracellular amount of mitoxantrone as described in the Experimental Section. Values were determined by using eq 1 and fitted with eq 2, as described in the Experimental Section. Squares and circles correspond to **1** and **15**, respectively.

Inhibition Mechanism of 15. As mentioned above, the R and H drug-transport sites were identified on P-gp, the former involved in the binding of rhodamine 123 and anthracyclines such as daunorubicin while the latter binds Hoechst 33342, colchicine, and quercetin.[15] We examined the behavior of **15** toward these drug-transport sites, monitoring with flow cytometry the variation of intracellular retention of daunorubicin and Hoechst 33342 in cells expressing P-gp. As detailed in the Experimental Section, substrates were used in the range of 0−20 μM for daunorubicin and 0−10 μM for Hoechst 33342. **15** was added at fixed concentrations of 0.11, 0.22, 0.33, and 1 μM. The resulting retention rates of substrates are displayed in Figure 5 as a direct function of substrate concentrations (panels A and C)

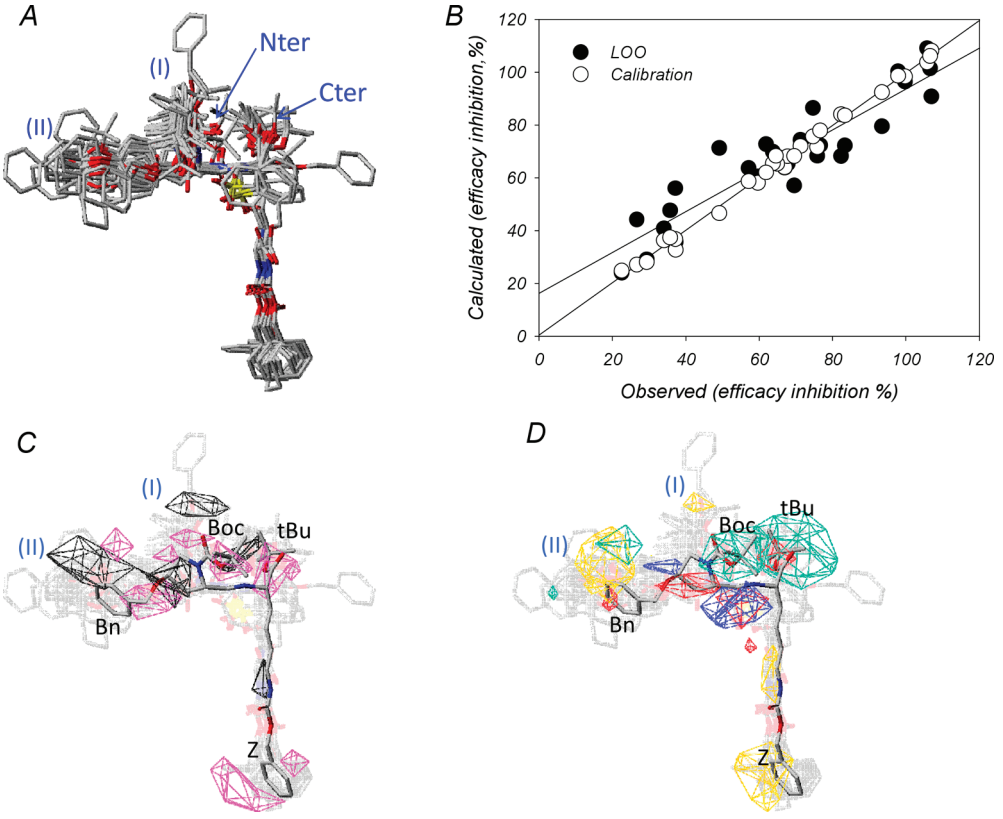

Figure 2. 3D-QSAR of the reversin-derived compounds CT. (A) Superimposed molecules of the series. Molecules were superimposed as detailed in the text. The regions labeled I and II are detailed in the corresponding paragraph in the Results and Discussion section. (B) Predicted versus experimental inhibition efficacy values. Calculated values (closed circles) were obtained with the CoMSIA model by the LOO method as described in the Experimental Section, with a correlation coefficient q^2_{cv} of 0.85, a line intercept of 16.29, and a slope of 0.77. Calculated values (open circles) were obtained with the CoMSIA model without validation method (calibration), as described in the Experimental Section, with a linear fit correlation coefficient r^2 of 0.99, a line intercept of 0.40, and a slope of 0.99. (C, D) Analyses of hydrophobic (C) and electrostatic and steric (D) clusters. They were carried out as described in the Experimental Section and displayed is the structure of the most efficient compound **15**, the remaining derivatives being shown as a ghost. Favorable and unfavorable characters were as follows: pink and black clusters, respectively, for hydrophobicity, red and blue clusters for the electrostatic field and yellow and green for the steric field.

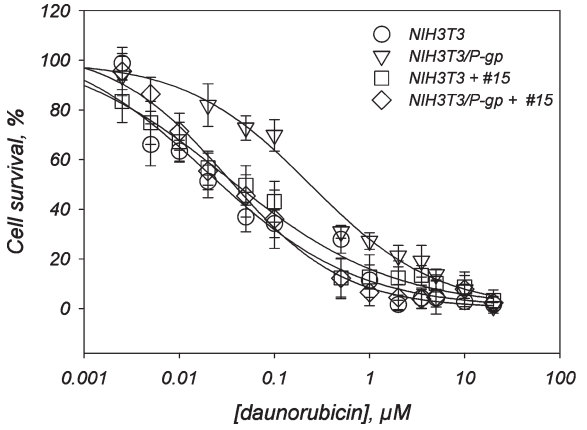

Figure 3. P-gp-expressing cells chemosensitization by **15**. Chemosensitization was assayed and quantified as described in the Experimental Section, using daunorubicin as anticancer drug at indicated concentrations and with **15** added at 1 μM. Complete cell survival (100%) was estimated as the number of cells in absence of anticancer drug. Squares and circles correspond to control NIH3T3 cells that do not express P-gp incubated with and without **15**, respectively. Triangles and diamonds correspond to the same conditions with NIH3T3/P-gp cells.

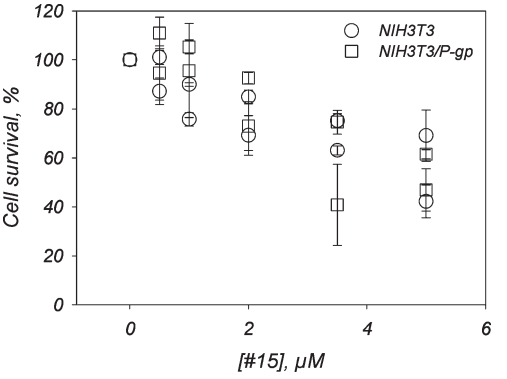

Figure 4. Cytotoxicity of **15**. The compound was added at the indicated concentrations. Complete cell survival (100%) was estimated as the number of cells in the absence of compound. Squares and circles correspond to experiments carried out with NIH3T3/P-gp and NIH3T3 cells, respectively.

or in Lineweaver−Burk double reciprocal plots[31] (panels B and D). As shown, the maximal retention rates appeared much more affected than the corresponding K_M. Fitting of the Lineweaver−Burk plots tend to a common intercept on the negative x-axis, $[drug]^{-1}$. Table 5 summarizes the kinetic parameters deduced from the direct plots by using the Michaelis and Menten equation. As shown, the Michaelis constant of each drug did not change while the corresponding maximal retention rates increased with the inhibitor concentration. All these data suggest that **15** behaves as a noncompetitive inhibitor toward both substrates. They allow to estimate K_I values of about 0.5 and 1.5 μM (Table 5), suggesting existence of a second, noncompetitive binding site for **15** at high concentration. Further docking experiments on P-gp will be carried out based on the mouse P-gp 3D structure[14] to localize the putative inhibitor binding sites.

Experimental Section

Chemistry. Solvents and reagents were of reagent grade and used without further purification. Melting points were taken on an Electrothermal 9200 apparatus or a Kofler bench and are uncorrected. Specific rotation $[\alpha]_D$ was recorded on Bellingham + Stanley Ltd. ADP 220, Jasco P-1010 or Roussel-Jouan 71 polarimeters. IR spectra were determined on Perkin-Elmer Spectrum One FT-IR or Perkin-Elmer 1600 series FT-IR spectrometers (KBr film). ^{1}H, ^{13}C, and ^{19}F NMR spectra were measured on Bruker AC 200 (^{1}H 200.11 MHz; ^{13}C 50.29 MHz), Bruker ALS 300 (^{1}H 300.17 MHz), Bruker AM 300 (^{1}H 300.17 MHz), or Bruker DRX 300 (^{13}C 75.44 MHz; ^{19}F 282.23 MHz) spectrometers (residual protonated solvent signal as internal reference). Elemental analysis was performed on all tested compounds by the Service Central d'Analyse, Vernaison, France, and the results, unless otherwise indicated in the Experimental Section, are within ±0.4% of theoretical values. Electrospray mass spectra were recorded on a Thermo-Finnigan LCQ-Advantage in dichloromethane. Column chromatography was carried out with Merck silica gel 60 (40−63 Å) or SDS silica gel 60 (35−70 Å).

(3*S*)-*tert*-Butoxycarbonylamino-4-oxohexanedioic Acid 6-Allyl Ester 1-Benzyl Ester (25). Carbonyldiimidazole (220 mg, 1.312 mmol) was added at room temperature to a stirred solution of N^{α}-Boc-Asp(OBn)-OH (404.5 mg, 1.25 mmol) in dry THF (6 mL) under argon atmosphere. The resulting solution was stirred for 1 h at the same temperature and used for the next step without further purification. Meanwhile, a solution of lithium enolate of allyl acetate was made by addition of 2.5 M BuLi solution in hexane (1.75 mL, 4.375 mmol) to a solution of diisopropylamine (615 μL, 4.375 mmol) in dry THF (6 mL) at 0 °C under argon atmosphere. The solution was stirred for 10 min at 0 °C and then cooled to −78 °C. A solution of allyl acetate (472 μL, 4.375 mmol) in THF (3 mL) was then added dropwise, and the resulting solution was stirred for 15 min at −78 °C. The above imidazole solution was added dropwise to the pale-yellow solution of lithium enolate at −78 °C under argon atmosphere. The resulting mixture was stirred for 2 h and then quenched at −78 °C with 1 M HCl (20 mL) and extracted with ethyl acetate (3 × 30 mL). The organic extracts were combined, washed with saturated sodium bicarbonate solution (2 × 40 mL) and brine (40 mL), dried over anhydrous sodium sulfate, filtered, and concentrated to provide the crude product as a yellow oil which was purified by flash chromatography on silica gel (petroleum ether/ethyl acetate 8:2) to afford 163 mg of **25** (32% yield) as a beige solid. Mp 48−51 °C. IR (film, cm^{-1}): 3371 (ν_{NH}), 2978 (ν_{CH}), 1733 ($\nu_{C=O}$), 1456 ($\nu_{\varphi C=C}$), 1392 1367 (δ_{CH3} *t*-Bu), 1167 ($\nu_{O-C-C\ asym}$). ^{1}H NMR (300 MHz, $CDCl_3$, δ): 1.38 (s, $-C(CH_3)_3$ Boc, 9H), 2.74 (dd, J = 4.6 and 17.8 Hz, CH_β, 1H), 2.98 (dd, J = 4.8 and 17.3 Hz, CH_β, 1H), 3.59 (s, CH_2-CO_2allyl, 2H), 4.53 (m, CH_α, 1H), 4.55 (dd, J = 1.8 and 6.7 Hz, $CH_2-CH=CH_2$, 2H), 5.05 (s, CH_2Ph, 2H), 5.23 (m, $CH=CH_2$, 2H), 5.57 (d, J = 9.0 Hz, N*H*, 1H), 5.83 (m, $CH=CH_2$, 1H), 7.28 (m, ArH, 5H).

(2*S*)-*tert*-Butoxycarbonylaminosuccinic Acid 1-Allyl Ester 4-Benzyl Ester (26). The product **26** is a byproduct issued from the synthesis of β-keto allyl ester **25**. This product (95 mg, 21% yield) was isolated by flash chromatography on silica gel (petroleum ether/ethyl acetate 8:2) as a yellow oil. IR (film, cm^{-1}): 3354 (ν_{NH}), 2935 (ν_{CH}), 1731 ($\nu_{C=O}$), 1447 ($\nu_{\varphi C=C}$), 1391 1366 (δ_{CH3} *t*-Bu), 1152 ($\nu_{O-C-C\ asym}$). ^{1}H NMR (300 MHz, $CDCl_3$, δ): 1.46 (s, $-C(CH_3)_3$ Boc, 9H), 2.89 (dd, J = 4.7 and 17.5 Hz, CH_β, 1H), 3.08 (dd, J = 5.0 and 16.7 Hz, CH_β, 1H), 4.60−4.68 (m, CH_α and $CH_2-CH=CH_2$, 3H), 5.14 (s, CH_2Ph, 2H), 5.28 (m, $CH=CH_2$, 2H), 5.50 (d, J = 7.9 Hz, N*H*, 1H), 5.87 (m, $CH=CH_2$, 1H), 7.36 (m, ArH, 5H).

6-Benzyloxycarbonylamino-(2*S*)-hydroxyhexanoic Acid (27). Commercial H-Lys(Z)-OH (1.012 g, 3.614 mmol) was dissolved in 50% aqueous acetic acid (120 mL). A solution of sodium nitrite (2 g, 29 mmol) in water (20 mL) was then added at 0 °C, and the reaction mixture was stirred for 40 min at the same temperature and then quenched with water (140 mL) and extracted with ethyl acetate (2 × 140 mL). The organic extracts

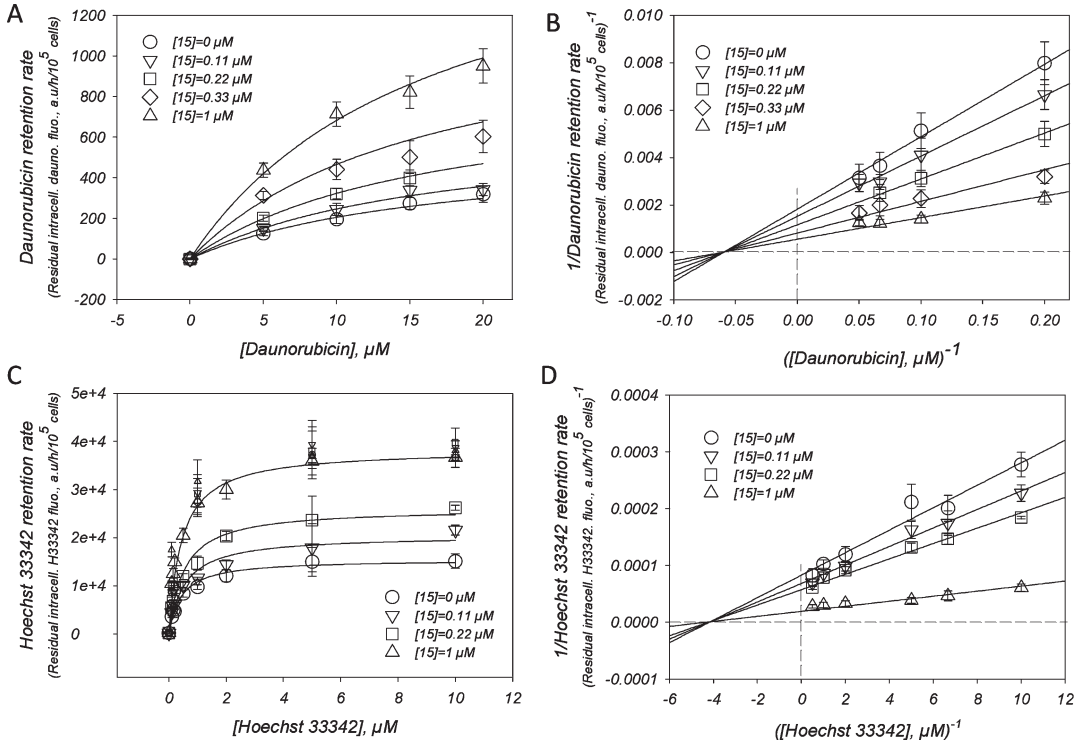

Figure 5. Compound **15** is a noncompetitive inhibitor of H and R drug-transport sites. Experiments were carried out as described in the Experimental Section and in Figure 1, using daunorubicin (A, B) and Hoechst 33342 (C, D) as transported drugs.[15] **15** was either omitted (0% inhibition, circles) or added at 0.11, 0.22, 0.33, and 1 μM corresponding to 25% (bottom-up triangles), 50% (squares), 75% (diamonds), and 100% (bottom-down triangles) inhibition respectively, as deduced from Figure 2. The drug retention rate corresponding to the amount of drug (expressed as arbitrary units of fluorescence, a.u.) remaining inside 10^5 cells after 1 h was plotted as a function of drug concentration (A, C) and fitted with the Michaelis and Menten equation data. Small symbols in panel C correspond to the same series of experiments, carried out with control NIH3T3 cells. Data are also displayed in Lineweaver−Burk double-reciprocal plots[31] (B, D). Experiments were carried out in duplicate in two independent series.

Table 5. Kinetic Inhibition Parameters of **15**[a]

[**15**], μM	R_{max}	K_M, μM	K_I, μM
	Daunorubicin Substrate		
0	547 ± 42	16.7 ± 1.1	
0.11	656 ± 46	16.7 ± 1.2	0.66 ± 0.01
0.22	860 ± 65	16.4 ± 1.4	0.60 ± 0.01
0.33	1230 ± 58	15.9 ± 1.7	0.59 ± 0.04
1.0	1808 ± 77	16.3 ± 1.2	1.43 ± 0.08
	Hoechst 33342 Substrate		
0	15491 ± 562	0.23 ± 0.06	
0.11	20485 ± 1199	0.24 ± 0.12	0.45 ± 0.04
0.22	26098 ± 1278	0.27 ± 0.09	0.54 ± 0.06
1.0	38349 ± 987	0.25 ± 0.07	1.68 ± 0.08

[a] Maximal retention rates (R_{max}) and Michaelis constants (K_M) of daunorubicin and Hoechst 33342, as well as inhibition constants (K_I), were estimated from Figure 5, panels A and C, as described in the Experimental Section.

were combined, washed with 0.1 M HCl solution (200 mL), dried over anhydrous sodium sulfate, filtered, and concentrated to provide the crude product **27** (1 g, quantitative yield) as a yellow oil which was dried under vacuum in order to eliminate the remaining acetic acid and used without further purification. IR (film, cm^{-1}): 3454 3335 (ν_{NH}, ν_{OH}, and ν_{COOH}), 2925 (ν_{CH}), 1683 ($\nu_{C=O}$), 1586, 1539, 1456 ($\nu_{\varphi C=C}$), 1260 (ν_{C-OH}), 1127 ($\nu_{O-C-C\ asym}$), 1102 (ν_{C-N}). ^{1}H NMR (300 MHz, $CDCl_3$, δ): 1.40−1.59 (m, C$H_{2\gamma}$, C$H_{2\delta}$, 4H), 1.82 (m, C$H_{2\beta}$, 2H), 3.22 (q, J = 6.4 Hz, CH_2N, 2H), 4.28 (m, CH_α, 1H), 4.94 (br, NH, 1H), 5.11 (s, CH_2Ph, 2H), 5.40−5.60 (br, COOH, 1H), 7.36 (s, ArH, 5H).

6-Benzyloxycarbonylamino-(2*S*)-hydroxyhexanoic Acid Benzyl Ester (28). Acid **27** (1 g, 3.56 mmol) was dissolved in acetone (20 mL), and triethylamine (600 μL, 4.27 mmol) was added. Benzyl bromide (510 μL, 4.27 mmol) was then added dropwise, and the reaction mixture was stirred for 6 h at room temperature. The solvent was evaporated, and the obtained residue was dissolved in ethyl acetate, washed with saturated sodium bicarbonate solution and brine (twice each one), dried over anhydrous sodium sulfate, filtered, and concentrated. The yellow oily residue was purified by flash chromatography on silica gel (petroleum ether/ethyl acetate 6:4) to yield 516 mg of **28** (40% yield) as a yellow oil. IR (film, cm^{-1}): 3365 (ν_{NH} and ν_{OH}), 3066, 3034 ($\nu_{\varphi CH}$), 2937 (ν_{CH}), 1738 1699 ($\nu_{C=O}$), 1587, 1538, 1455 ($\nu_{\varphi C=C}$), 1251 ($\nu_{C-C-O\ asym}$), 1126 ($\nu_{O-C-C\ asym}$). ^{1}H NMR (300 MHz, $CDCl_3$, δ): 1.27−1.89 (m, C$H_{2\beta}$, C$H_{2\gamma}$, C$H_{2\delta}$, 6H), 3.17 (q, J = 6.4 Hz, CH_2N, 2H), 4.23 (m, CH_α, 1H), 4.75 (br, NH, 1H), 5.10 (s, CH_2Ph, 2H), 5.20 (AB, J = 12.4 Hz, CH_2Ph, 2H), 7.36 (m, 2ArH, 10H).

6-Benzyloxycarbonylamino-(2*S*)-trifluoromethanesulfonyloxyhexanoic Acid Benzyl Ester (29). Alcohol **28** (302.7 mg, 0.816 mmol) was dissolved in CH_2Cl_2 (5 mL) and then cooled to −78 °C (acetone). 2,6-Lutidine (265 μL, 2.284 mmol) was added dropwise followed by triflic anhydride (276 μL, 1.632 mmol). The resulting solution was allowed to warm to room temperature and the reaction mixture was stirred under argon for 4 h. An amount of 5 g of silica gel was added directly to the reaction before evaporation of the solvent at room temperature under reduced pressure. Purification by flash chromatography on silica gel (petroleum ether/ethyl acetate 8:2) afforded 170 mg of **29** (41% yield) as a brownish oil. IR (film, cm^{-1}): 3349 (ν_{NH}), 3068, 3036 ($\nu_{\varphi CH}$), 2942 (ν_{CH}), 1760, 1715 ($\nu_{C=O}$), 1587, 1456, 1417 ($\nu_{\varphi C=C}$), 1326 ($\nu_{SO2\ asym}$), 1246 ($\nu_{C-C-O\ asym}$), 1144 ($\nu_{SO2\ sym}$), 698 (ν_{CF3}). ^{1}H NMR (300 MHz, $CDCl_3$, δ): 1.36−1.59 (m, C$H_{2\gamma}$, C$H_{2\delta}$, 4H), 2.03 (m, C$H_{2\beta}$, 2H), 3.17 (q, J = 6.5 Hz, CH_2N, 2H), 4.71

(br, N*H*, 1H), 5.11 (s, CH_2Ph, 2H), 5.14 (m, CH_α, 1H), 5.27 (AB, J = 12.0 Hz, CH_2Ph, 2H), 7.36 (m, 2ArH, 10H). ^{19}F NMR (282 MHz, $CDCl_3$, δ): −75 (CF_3).

N^α-Boc-(*S*)-Asp(OBn)-ψ(CO-CH$_2$)-(*S*)-Lys(Z)-OBn (30). A solution of **25** (119 mg, 0.294 mmol) in dry THF (2 mL) was added dropwise to a stirred suspension of NaH (14 mg of 60% in oil, 0.353 mmol) in dry THF (2 mL) at −20 °C under argon. The mixture was stirred for 20 min. Then the alkyl triflate **29** (162.7 mg, 0.323 mmol) in dry THF (1 mL) was added. The resulting solution was allowed to warm to room temperature and stirred for 3 h. After being quenched with 1 M HCl (5 mL), the reaction mixture was then extracted with ethyl acetate (3 × 10 mL). The organic extracts were combined, washed with saturated sodium bicarbonate solution (15 mL) and brine (15 mL), dried over anhydrous sodium sulfate, passed through a short pad of silica gel, and concentrated to provide a yellow oil. Without further purification, this oil (223 mg, 0.294 mmol) was dissolved in dry THF (2 mL) and added dropwise to a stirred solution of palladium acetate (1.6 mg, 7.23.10^{-3} mmol), PPh_3 (3.9 mg, 0.0147 mmol), formic acid (22 μL, 0,588 mmol), and Et_3N (105 μL, 0.735 mmol) in dry THF (2 mL) at room temperature under argon. The mixture was stirred overnight. After the solvent was evaporated under reduced pressure, the oily residue was purified by flash chromatography on silica gel (petroleum ether/ethyl acetate 7:3) to afford 52 mg of **30** (26% yield) as a brown oil. $[\alpha]^{25}_D$ −10.0 (*c* 0.19, CH_2Cl_2). IR (film, cm^{-1}): 3360 (ν_{NH}), 3034 ($\nu_{\varphi CH}$), 2933 (ν_{CH}), 1715 ($\nu_{C=O}$), 1587, 1456 ($\nu_{\varphi C=C}$), 1367 (δ_{CH3} *t*-Bu), 1251 ($\nu_{C-C-O\ asym}$), 1165 ($\nu_{O-C-C\ asym}$). ^{1}H NMR (300 MHz, $CDCl_3$, δ): 1.37 (s, C(CH_3)$_3$ Boc, 9H), 1.10−1.72 (m, 3CH_2 Lys, 6H), 2.45−2.91 (m, CH_2CO, CH_2CO$_2$Bn, 4H), 3.05 (q, J = 6.7 Hz, CH_2N, 2H), 4.38 (m, CH_α, 1H), 4.62 (m, CH_α, 1H), 4.97−5.16 (m, 3CH_2Ph, 6H), 5.45 (d, J = 8.3 Hz, N*H*, 1H), 7.22−7.29 (m, 3ArH, 15H). ^{13}C NMR ($CDCl_3$, 75 MHz): 28.7 (3C), 24.4, 30.0, 31.7 (3C), 36.1 (C), 40.3 (C), 40.9 (C), 41.1 (C), 56.3 (C), 67.0, 67.1, 67.2 (3C), 80.7 (C), 128.5, 128.7, 128.8, 128.9, 129.0, 130.2 (15C), 135.7, 136.3, 137.0 (3C), 155.8, 156.7 (2C), 171.4, 175.1 (2C), 206.9 (C). MS-ESI (m/z): 1371.2 [2M + Na]$^+$, 697.3 [M + Na]$^+$. HRMS-ESI (m/z): [M + Na]$^+$ calculated for $C_{38}H_{46}N_2O_9Na$, 697.3101; found, 697.30991.

Biology. Cell Cultures and Drug Efflux Assays. The inhibition of P-gp activity by the studied compounds was evaluated by their ability to prevent the efflux of daunorubicin, mitoxantrone, and Hoechst 33342 (Sigma-Aldrich) in either the K562/R7 drug-selected human cell line[32] or the NIH3T3 G185 transfected cell line (ATCC).[33] They were also assayed on human embryonic kidney (HEK) 293 cells transfected with BCRP/ABCG2[34] and baby hamster kidney (BHK) 21 expressing MRP1.[35] K562/R7 cells (1 × 10^6 cells) were incubated for 1 h at 37 °C in 1 mL of RPMI 1640 medium containing a final concentration of 10 μM daunorubicin, in the presence or absence of 10 μM reversin derivatives. After incubation, cells were washed with ice-cold PBS and kept on ice until analysis by flow cytometry. Cyclosporin A was used as a positive control (mean inhibitory activity of 100%). NIH3T3 drug-sensitive parental cell line and its derivative cell line transfected with human MDR1-G185, NIH3T3/P-gp, derived from NIH Swiss mouse embryo cultures, were grown in Dulbecco's modified Eagle's medium (PAA laboratories) supplemented with 10% fetal bovine serum (PAA laboratories) and 1% penicillin/streptomycin (PAA Laboratories). The NIH3T3/P-gp growth medium was also supplemented with 60 ng/mL colchicine. Cells were incubated at 37 °C in humidified 5% CO_2. NIH3T3 and NIH3T3/P-gp were incubated for 30 min at 37 °C under 5% CO_2 in the presence of 10 μM mitoxantrone or various concentrations of either daunorubicin or Hoechst 33342 (as indicated in Figures) as the P-gp transport substrate, with or without reversin derivatives. Compounds were solubilized in DMSO, the final concentration of which was limited to 0.5%. After incubation, cells were washed with phosphate buffer saline (PBS) (PAA Laboratories) and incubated for 1 h in the same media without drug; cells were maintained on ice until analysis by flow cytometry.

Flow Cytometry. The fluorescence of intracellular daunorubicin or mitoxantrone was measured with a Facscan flow cytometer (Becton Dickinson, Mountain View, CA). Daunorubicin and mitoxantrone were excited at 488 nm, and the fluorescence emission was monitored at 650 nm. The amount of Hoechst 33342 was measured by a LSRII flow cytometer, at 350 nm excitation and 450 nm emission. The compound efficiency was estimated by using eq 1,

$$\%\ \text{efficacy} = 100 \times (\text{FA} - \text{FBG})/(\text{Fe} - \text{FBG}) \qquad (1)$$

where FA and FBG (background) correspond to the intracellular fluorescence of cells expressing P-gp incubated with (FA) or without (FBG) the fluorescent transported drug, in the presence of each tested compound, Fe corresponding to FA measured on control cells that do not express P-gp. Assays were performed in duplicate. Mean and standard error (SE) were calculated from at least three independent experiments, and curves were fitted with Sigmaplot using the eq 2:

$$\%\ \text{efficacy} = a(1 - \exp(-b[\text{inhibitor},\ \mu\ \text{M}])) \qquad (2)$$

a and b parameters being adjusted by the fit.

Cytotoxicity Assays. Cells were seeded in 200 μL of growth medium at a density of 2500 cells per well in a 96-well plate and were allowed to establish for 24 h at 37 °C in humidified 5% CO_2. The medium was then removed, replaced by 100 μL of growth medium, completed with 100 μL of each tested compound at increasing concentrations in 1% DMSO. Cells were incubated for 72 h at 37 °C in humidified 5% CO_2. The cytotoxicity of each tested compounds was then evaluated with a 3-(4,5-dimethylthiazol-2-yl)-2,5-diphenyltetrazolium bromide (MTT) colorimetric assay (Sigma-Aldrich).

Chemosensitization Assays. Experiments were carried as for cytotoxicity assays, incubating control or P-gp-expressing cells with increasing concentrations of anticancer drugs as indicated and a concentration of the tested modulator corresponding to 5 times its IC_{50}.

Kinetics. Kinetic parameters for P-gp inhibition by compound **15** were determined by incubating 10^5 NIH3T3/P-gp and NIH3T3 cells with various concentrations of daunorubicin (5, 10, 15, and 20 μM) in the presence of four to five concentrations (0, 0.11, 0.22, 0.33, and 1 μM) of **15**. The residual intracellular amount of drugs remaining inside cells after 1 h of incubation with or without **15** was quantified by fluorescence coupled to flow cytometry at each concentration of **15**, with data proportional to a drug retention rate. It was plotted as a function of drug concentration (A, C) and fitted with the Michaelis and Menten equation $R = R_{max}[D]/([D] + K_M)$ where R is the drug retention rate, R_{max} the maximal drug retention rate, [D] the drug concentration, and K_M the Michaelis constant of drug efflux. The inhibition constant of **15**, K_I was deduced from the equation $R_{max}' = R_{max}/(1 + [I]/K_I)$, where R_{max}' corresponds to the maximal drug retention rate calculated at each modulator concentration [I]. Each value is the mean of two duplicate experiments.

Bioinformatics. 3D-QSAR. Molecules were modeled with the Sybyl molecular-modeling package using the force field and partial charges of MMFF94.[36−39] The dielectric constant was set to 80 to simulate the solvent, and the electrostatic cut-off was set to 16 Å. In CoMSIA, the steric, electrostatic, hydrophobic, hydrogen bond donor, hydrogen bond acceptor, and donor−acceptor similarity index fields were calculated, with a default attenuation factor of 0.3 in a grid box extended by adding 6 Å to the largest model, in all directions of the space. A common probe atom was used, with 1 Å radius and charge, hydrophobicity, and hydrogen bond properties of +1. The indices were evaluated according to the usual CoMSIA protocol with a 2.0 kcal·mol^{-1} column filtering value. The predictive power of the models was

evaluated by LOO cross-validation (SYBYL 6.9−7.3 versions; Tripos Inc.) based on the cross-validated coefficient (q^2), displayed in Figure 2B, finding an optimal component number of 10. The maximal error of prediction is about 22% of inhibition with a mean error value of 5.2% ± 6.1.

Acknowledgment. We thank Léa Payen (Institut des Sciences Pharmaceutiques et Biologiques, Lyon, France) for critical discussion and Philippe Lawton (Institut des Sciences Pharmaceutiques et Biologiques, Lyon, France) for proofreading. This work was supported by the Centre National de la Recherche Scientifique (CNRS) and University of Lyon 1 (UMR5086), and the French Ministry of Research (EA3741, Lyon 1). It was funded by the National Research Agency (Grants ANR-06-BLAN_0420, ANR-06-PCVI-0019-01, ANR piribio09_444706), the Association pour la Recherche sur le Cancer (ARC), and the Ligue Nationale Contre le Cancer (Labellisation 2009). The Ph.D. fellowship of Ophélie Arnaud was from the French Ministry of Research.

Supporting Information Available: Synthetic procedures and analytical data for compounds **1**−**24**; example of estimation of the inhibition efficacy by flow cytometry. This material is available free of charge via the Internet at http://pubs.acs.org.

References

(1) Dean, M.; Hamon, Y.; Chimini, G. The human ATP-binding cassette (ABC) transporter superfamily. *J. Lipid Res.* **2001**, *42*, 1007–1017.
(2) Mourez, M.; Jéhanno, M.; Hofnung, M.; Dassa, E. Rôle, fonctionnement et structure des transporteurs à ATP binding cassette (ABC). *Med. Sci.* **2000**, *16*, 386–94.
(3) Kim, R. B. Drug transporters in HIV Therapy. *Top. HIV Med.* **2003**, *11*, 136–139.
(4) Wang, X.; Furukawa, T.; Nitanda, T.; Okamoto, M.; Sugimoto, Y.; Akiyama, S.; Baba, M. Breast cancer resistance protein (BCRP/ABCG2) induces cellular resistance to HIV-1 nucleoside reverse transcriptase inhibitors. *Mol. Pharmacol.* **2003**, *63*, 65–72.
(5) Weiss, J.; Rose, J.; Storch, C. H.; Ketabi-Kiyanvash, N.; Sauer, A.; Haefeli, W. E.; Efferth, T. Modulation of human BCRP (ABCG2) activity by anti-HIV drugs. *J. Antimicrob. Chemother.* **2007**, *59*, 238–245.
(6) Juliano, R. L.; Ling, V. A surface glycoprotein modulating drug permeability in Chinese hamster ovary cell mutants. *Biochim. Biophys. Acta, Biomembr.* **1976**, *455*, 152–162.
(7) Cole, S. P.; Bhardwaj, G.; Gerlach, J. H.; Mackie, J. E.; Grant, C. E.; Almquist, K. C.; Stewart, A. J.; Kurz, E. U.; Duncan, A. M.; Deeley, R. G. Overexpression of a transporter gene in a multidrug-resistant human lung cancer cell line. *Science* **1992**, *258*, 1650–1654.
(8) Doyle, L. A.; Yang, W.; Abruzzo, L. V.; Krogmann, T.; Gao, Y.; Rishi, A. K.; Ross, D. D. A multidrug resistance transporter from human MCF-7 breast cancer cells. *Proc. Natl. Acad. Sci. U.S.A.* **1998**, *95*, 15665–15670.
(9) Litman, T.; Brangi, M.; Hudson, E.; Fetsch, P.; Abati, A.; Ross, D. D.; Miyake, K.; Resau, J. H.; Bates, S. E. The multidrug-resistant phenotype associated with overexpression of the new ABC half-transporter, MXR (ABCG2). *J. Cell Sci.* **2000**, *113* (Part 11), 2011–2021.
(10) Pascaud, C.; Garrigos, M.; Orlowski, S. Multidrug resistance transporter P-glycoprotein has distinct but interacting binding sites for cytotoxic drugs and reversing agents. *Biochem. J.* **1998**, *333* (Part 2), 351–358.
(11) Martin, C.; Berridge, G.; Higgins, C. F.; Mistry, P.; Charlton, P.; Callaghan, R. Communication between multiple drug binding sites on P-glycoprotein. *Mol. Pharmacol.* **2000**, *58*, 624–632.
(12) Colabufo, N. A.; Berardi, F.; Cantore, M.; Contino, M.; Inglese, C.; Niso, M.; Perrone, R. Perspectives of P-glycoprotein modulating agents in oncology and neurodegenerative diseases: pharmaceutical, biological, and diagnostic potentials. *J. Med. Chem.* **2009**, *53*, 1883–1897.
(13) Garrigues, A.; Loiseau, N.; Delaforge, M.; Ferté, J.; Garrigos, M.; André, F.; Orlowski, S. Characterization of two pharmacophores on the multidrug transporter P-glycoprotein. *Mol. Pharmacol.* **2002**, *62*, 1288–1298.
(14) Aller, S. G.; Yu, J.; Ward, A.; Weng, Y.; Chittaboina, S.; Zhuo, R.; Harrell, P. M.; Trinh, Y. T.; Zhang, Q.; Urbatsch, I. L.; Chang, G. Structure of P-glycoprotein reveals a molecular basis for poly-specific drug binding. *Science* **2009**, *323*, 1718–1722.
(15) Shapiro, A. B.; Ling, V. Positively cooperative sites for drug transport by P-glycoprotein with distinct drug specificities. *Eur. J. Biochem.* **1997**, *250*, 130–137.
(16) Avendano, C.; Menendez, J. C. Inhibitors of multidrug resistance to antitumor agents (MDR). *Curr. Med. Chem.* **2002**, *9*, 159–193.
(17) Teodori, E.; Dei, S.; Martelli, C.; Scapecchi, S.; Gualtieri, F. The functions and structure of ABC transporters: implications for the design of new inhibitors of Pgp and MRP1 to control multidrug resistance (MDR). *Curr. Drug Targets* **2006**, *7*, 893–909.
(18) Szakacs, G.; Paterson, J. K.; Ludwig, J. A.; Booth-Genthe, C.; Gottesman, M. M. Targeting multidrug resistance in cancer. *Nat. Rev. Drug Discovery* **2006**, *5*, 219–234.
(19) Seprödi, J.; Mezõ, I.; Vadász, Z.; Szabó, K.; Sarkadi, B.; Teplán, I. *Peptides Derivatives against Multidrug Resistance*: Mayflower Scientific Ltd.: Kingswinford, U.K., 1998.
(20) Vadász, Z.; Szabó, K.; Sarkadi, B.; Teplán, I.; Mák, M.; Miklós, I.; Györffy, E.; Seprödi, J. New Hydrophobic Peptide-like Compounds Modulating MDR1-ATPase Activity. *Proceedings of the 25th European Peptide Symposium*; Bajusz, S., Hudecz, F., Eds.; Akadémiai Kiadó: Budapest, Hungary, 1999; pp 640−641.
(21) Sharom, F. J.; Yu, X.; Lu, P.; Liu, R.; Chu, J. W.; Szabo, K.; Muller, M.; Hose, C. D.; Monks, A.; Varadi, A.; Seprodi, J.; Sarkadi, B. Interaction of the P-glycoprotein multidrug transporter (MDR1) with high affinity peptide chemosensitizers in isolated membranes, reconstituted systems, and intact cells. *Biochem. Pharmacol.* **1999**, *58*, 571–86.
(22) Koubeissi, A.; Raad, I.; Ettouati, L.; Guilet, D.; Dumontet, C.; Paris, J. Inhibition of P-glycoprotein-mediated multidrug efflux by aminomethylene and ketomethylene analogs of reversins. *Bioorg. Med. Chem. Lett.* **2006**, *16*, 5700–5703.
(23) Charrier, C.; Ettouati, L.; Paris, J. New application of the Julia olefination for the synthesis of Tyr-Gly E-alkene and carba isostere pseudopeptides. *Tetrahedron Lett.* **1999**, *40*, 5705–5707.
(24) Lai, M. Y. H.; Brimble, M. A.; Callis, D. J.; Harris, P. W. R.; Levi, M. S.; Sieg, F. Synthesis and pharmacological evaluation of glycine-modified analogues of the neuroprotective agent glycyl-l-prolyl-l-glutamic acid (GPE). *Bioorg. Med. Chem.* **2005**, *13*, 533–548.
(25) Martinez, J.; Bali, J. P.; Rodriguez, M.; Castro, B.; Magous, R.; Laur, J.; Lignon, M. F. Synthesis and biological activities of some pseudo-peptide analogs of tetragastrin: the importance of the peptide backbone. *J. Med. Chem.* **1985**, *28*, 1874–1879.
(26) Hoffman, R. V.; Tao, J. Synthesis of Cbz-Protected Ketomethylene Dipeptide Isosteres. In *Peptidomimetics Protocols*; Kazmierski, W. M., Ed.; Methods in Molecular Medecine, Vol. 23; Humana Press: Totowa, NJ, 1999; pp 106−121.
(27) Shin, I.; Lee, M.; Lee, J.; Jung, M.; Lee, W.; Yoon, J. Synthesis of optically active phthaloyl D-aminooxy acids from L-amino acids or L-hydroxy acids as building blocks for the preparation of aminooxy peptides. *J. Org. Chem.* **2000**, *65*, 7667–75.
(28) Yang, D.; Li, B.; Ng, F. F.; Yan, Y. L.; Qu, J.; Wu, Y. D. Synthesis and characterization of chiral N−O turns induced by alpha-aminoxy acids. *J. Org. Chem.* **2001**, *66*, 7303–12.
(29) Weber, I.; Potier, P.; Thierry, J. Triflates as synthons for the synthesis of lysine analogues. *Tetrahedron Lett.* **1999**, *40*, 7083–7086.
(30) Hoffman, R. V.; Maslouh, N.; Cervantes-Lee, F. Highly stereoselective syntheses of syn- and anti-1,2-amino alcohols. *J. Org. Chem.* **2001**, *67*, 1045–1056.
(31) Lineweaver, H.; Burk, D. The determination of enzyme dissociation constants. *J. Am. Chem. Soc.* **1934**, *56*, 658–666.
(32) Comte, G.; Daskiewicz, J.-B.; Bayet, C.; Conseil, G.; Viornery-Vanier, A.; Dumontet, C.; Di Pietro, A.; Barron, D. C-Isoprenylation of flavonoids enhances binding affinity toward P-glycoprotein and modulation of cancer cell chemoresistance. *J. Med. Chem.* **2001**, *44*, 763–768.
(33) Cardarelli, C. O.; Aksentijevich, I.; Pastan, I.; Gottesman, M. M. Differential effects of P-glycoprotein inhibitiors on NIH3T3 cells transfected with wild-type (G185) or mutant (V185) multidrug transporters. *Cancer Res.* **1995**, *55*, 1086–1091.
(34) Robey, R. W.; Steadman, K.; Polgar, O.; Morisaki, K.; Blayney, M.; Mistry, P.; Bates, S. E. Pheophorbide a is a specific probe for ABCG2 function and inhibition. *Cancer Res.* **2004**, *64*, 1242–1246.
(35) Chang, X.-B.; Hou, Y.-X.; Riordan, J. R. ATPase activity of purified multidrug resistance-associated protein. *J. Biol. Chem.* **1997**, *272*, 30962–30968.

(36) Halgren, T. A. Merck molecular force field. I. Basis, form, scope, parameterization, and performance of MMFF94. *J. Comput. Chem.* **1996**, *17*, 490–519.
(37) Halgren, T. A. Merck molecular force field. II. MMFF94 van der Waals and electrostatic parameters for intermolecular interactions. *J. Comput. Chem.* **1996**, *17*, 520–552.
(38) Halgren, T. A. Merck molecular force field. III. Molecular geometries and vibrational frequencies for MMFF94. *J. Comput. Chem.* **1996**, *17*, 553–586.
(39) Halgren, T. A.; Nachbar, R. B. Merck molecular force field. IV. conformational energies and geometries for MMFF94. *J. Comput. Chem.* **1996**, *17*, 587–615.